2005

Cryogenic Laser Induced U(VI) Fluorescence Studies of a U(VI) Substituted Natural Calcite: Implications to U(VI) Speciation in Contaminated Hanford Sediments

Zheming Wang
Pacific Northwest National Laboratory, Zheming.wang@pnl.gov

John M. Zachara
Pacific Northwest National Laboratory, john.zachara@pnl.gov

James Mckinley
Pacific Northwest National Laboratory, james.mckinley@pnl.gov

Steven Smith
Pacific Northwest National Laboratory, steven.smith@pnl.gov

Environ. Sci. Technol. **2005**, *39,* 2651−2659

Cryogenic Laser Induced U(VI) Fluorescence Studies of a U(VI) Substituted Natural Calcite: Implications to U(VI) Speciation in Contaminated Hanford Sediments

ZHEMING WANG,* JOHN M. ZACHARA, JAMES P. MCKINLEY, AND STEVEN C. SMITH

Pacific Northwest National Laboratory, Richland, Washington 99354

Time-resolved laser-induced fluorescence spectroscopy (TRLFS) and imaging spectromicroscopy (TRLFISM) were used to examine the chemical speciation of uranyl in contaminated subsurface sediments from the U.S. Department of Energy (U.S. DOE) Hanford Site, Washington. Spectroscopic measurements for contaminant U(VI) were compared to those from a natural, uranyl-bearing calcite (NUC) that had been found via X-ray absorption spectroscopy (XAS) to include uranyl in the same coordination environment as calcium. Spectral deconvolution of TRLFS measurements on the NUC revealed the unexpected presence of two distinct chemical environments consistent with published spectra of U(VI)-substituted synthetic calcite and aragonite. Apparently, some U(VI) substitution sites in calcite distorted to exhibit a local, more energetically favorable aragonite structure. TRLFS measurements of the Hanford sediments NP4−1 and NP1−6 were similar to the NUC in terms of peak positions and intensity, despite a small $CaCO_3$ content (1.0 to 3.2 mass %). Spectral deconvolution of the sediments revealed the presence of U(VI) in calcite and aragonite structural environments. A third, unidentified U(VI) species was also present in the NP1−6 sediment. TRLFISM measurements at multiple locations in the different sediments displayed only minor variation, indicating a uniform speciation pattern. Collectively, the measurements implied that waste U(VI), long-resident beneath the sampled disposal pond (32 y), had coprecipitated within carbonates. These findings have major implications for the solubility and fate of contaminant U(VI).

Introduction

The interaction of uranium with carbonate minerals, particularly the $CaCO_3$ polymorphs calcite and aragonite, has an important bearing on the mobility of contaminant uranium in near-surface environments. Carbonate minerals are among the most common secondary minerals formed in nature, and dissolved carbonate is a common component of waste solutions containing uranium. In the near surface, uranium is prevalently hexavalent and occurs as the uranyl ion, UO_2^{2+}, which forms strong carbonato complexes. The association of uranyl with carbonate minerals, either sorbed on the mineral surface or incorporated in the mineral structure through coprecipitation, could have a controlling influence on its mobility. In addition, the relative solubility and stability of carbonate minerals containing uranyl could determine its long-term availability for remobilization.

Spectroscopic studies have revealed a complex and as yet unresolved relationship between diverse mineral structures and adsorbed or substituted uranyl. Uranium may adsorb to mineral surfaces as the uranyl ion, UO_2^{2+}, but may also adsorb as a carbonato complex (e.g., Fe−Oxide- -UO_2^{2+}-CO_3^{2-} (*1*, *2*)). On calcite surfaces, uranyl tricarbonate-like adsorption complexes dominate at low solution concentrations, but surface precipitates of uranyl carbonate and hydroxide may form at higher concentrations (*3*). Multiple uranyl surface species are therefore likely to exist in contaminated near-surface environments.

The sorption of numerous metal ions on carbonate surfaces has been intensively studied (e.g., (*4*) and citations therein), and these studies illustrated the behavior of the carbonate surface in the presence of ions other than Ca^{2+}. The carbonate surface is more reactive than the surface of silicates or oxides, with sorption initiating the substitution of divalent cations for Ca^{2+}. The divalent metals coordinate differentially on the mineral surface at structurally distinct surface sites, substituting for Ca^{2+} in the surface layer (*5*, *6*), and the adjacent in-plane CO_3^{2-} ions in the host surface adjust to the radius of the substituting ion (*6*, *7*). As surface loading increases, the trace impurity is incorporated as a solid solution in the carbonate crystal lattice (*7*). Relatively large ions, such as Ba^{2+} and Pb^{2+}, which form discrete carbonate minerals only in the aragonite structure with 9-fold coordination with the carbonate ion, are known to substitute through crystal lattice distortion in octahedral coordination for Ca^{2+} in calcite. Distortion and relaxation of the carbonate lattice around the impurity ions are thus responsible for the wide range of isovalent substitutions observed in nature. The surface of the carbonate mineral is also chemically dynamic, reacting continuously with pore solutions and dissolved ions. In an experiment in which the calcite surface was exposed to Co^{2+} for 0.9 h, for instance, with no net carbonate deposition, Co was subsequently found to a depth of more than 10 μm (*4*).

The coprecipitation of uranyl with the carbonate minerals occurs with complex variations. The coordination environment in calcite, with a trigonal crystal structure, is distinct from that in aragonite, which is orthorhombic. The aragonite structure is more compatible with uranyl substitution than that of calcite, as indicated by the differences in observed solid−liquid distribution coefficients $(U/Ca_{solid})/(U/Ca_{liquid})$, for the two minerals; 1−10 for aragonite and 0.01−0.1 for calcite (*8*). In aragonite, uranyl exists in an equatorial coordination that is similar to the dominant aqueous species $[UO_2(CO_3)_3^{4-}]$, and this tricarbonate unit, in which uranyl is coordinated in a bidentate relationship with three carbonate ions, is incorporated in the mineral structure intact. In calcite, a change in coordination is necessary for uranyl coprecipitation, and the UO_2^{2+} ion has a disordered and less stable coordination environment (*9*). A study of natural calcite that contained ca. 360 mg of uranium kg^{-1} (*1*), showed that uranyl replaced Ca^{2+} and two carbonate ions in the calcite structure. This substitution resulted in UO_2^{2+} coordinating via four monodentate linkages with carbonate ions in the equatorial plane. Rapidly precipitated synthetic calcite specimens were

* Corresponding author phone: (509)376-6119; fax: (509)376-3650; e-mail: zheming.wang@pnl.gov. Corresponding author address: Pacific Northwest National Laboratory, P.O. Box 999, MSIN: K8-96, Richland, WA 99354.

10.1021/es048448d CCC: $30.25
Published on Web 03/11/2005

structurally more complex, and UO_2^{2+} was shown to have a coordination number of five, through either two bidentate linkages and one monodentate linkage to carbonate ions or through one bidentate linkage and three monodentate linkage to carbonate ions; these ions were in a coordination that was modified from the uranyl tricarbonate complex (*9*). Further study by the same researchers, involving experimental variations in the chemical conditions and precipitation rate for calcite, resulted in coexistent, multiple coordination environments within the calcite crystal structure, including a small tricarbonate [$UO_2(CO_3)_3^{4-}$] component (*10*). The spectroscopic investigation of uranyl substitution into calcite may thus rely on the ability to differentiate between species that resemble the aqueous tricarbonate or in which the coordination with carbonate ions has been modified.

The compositions of uranyl-bearing carbonates in nature, where slow reaction progress would be expected to produce uniform distributions of trace substituents, suggest that small environmental variations can control the incorporation of uranyl in the mineral structure. Research into uranium concentrations in marine calcite and aragonite (*11*−*13*) showed that the incorporation of uranyl was dependent on the concentrations of carbonate and of other ions, consistent with observations of the differential incorporation of uranium during crystal growth along different crystal faces (*10*), and the influence of trace Mg^{2+} on crystal growth (*14*). The chemistry of uranyl substitution in the carbonate mineral lattice will thus depend on the complex interplay of the system's composition and the kinetics of carbonate precipitation. Studies of contaminant uranyl in the presence of dissolved carbonate or coprecipitated in carbonate solid phases must therefore employ careful and detailed characterization methods.

In this study, we used liquid-helium-temperature time-resolved laser-induced fluorescence spectroscopy (TRLFS) and imaging spectromicroscopy (TRLFISM) to examine the crystallographic environment of uranyl in contaminated subsurface sediments. We contrasted those results to a natural, uranyl-bearing calcite (NUC) that had been studied previously (*1*). Our previous work (*15*, *16*) has shown that the fluorescence spectral intensity and resolution and fluorescence lifetime are greatly increased at near liquid helium (LHeT) temperatures, allowing identification of uranyl species in complex environmental samples for which weak, broad and featureless fluorescence spectra are usually observed at room temperature. TRLFS provided detailed information on the coordination of uranyl in the waste-impacted sediments and on comparative variations in coordination in the natural calcite that were not apparent from XAS fitting results.

Experimental Procedures

Sample Origin, Preparation, and Chemical Analyses. *U-Rich Natural Calcite Sample.* A uranium-rich natural calcite specimen (360 mg uranium kg^{-1}; NUC) was provided by Dr. N. C. Sturchio, Argonne National Laboratory, Argonne, IL. The calcite was retrieved from a 13 700 year-old speleothem deposit in the Vinschgau Valley of northernmost Italy (*17*). An X-ray diffraction analysis (*1*) indicated that the sample was > 99.8% pure calcite. For both spectroscopic and microscopic analyses, the solids were carefully scraped from a larger piece of calcite crystal of about 15 mm × 20 mm × 30 mm, and analyzed as received.

Hanford 300 Area Pond Sediments. Samples were collected as part of a larger effort to characterize and understand a uranium-contaminated site. Research and development operations and nuclear fuels fabrication activities at the U.S. Department of Energy (U.S. DOE) Hanford Site "300 Area" north of Richland, WA, from 1943 to 1975, generated liquid and solid wastes that were codisposed to adjacent infiltration ponds within 100 m of the Columbia River. Although the inventory of the disposal basins was incompletely documented, process wastes from nuclear fuel fabrication, various radioactive liquid wastes, sewage wastes, laboratory wastes, and coal power wastes were disposed to the infiltration basins. The volume and chemical inventories of the primary waste streams included basic sodium aluminate (15 wt % NaOH) from the dissolution of Al nuclear fuel cladding and nitric acid fuels-fabrication wastes containing U and Cu. The pH of the waste discharges to the ponds ranged intermittently from pH 2 to 11, depending on waste source. Sodium hydroxide was added to the ponds to neutralize low pH and to prevent metals migration to the nearby Columbia River. An estimate of the contaminant inventory disposed to the 300 Area North Process Pond included approximately 30 000 kg of dissolved U from enriched, natural, and depleted sources (*18*).

TABLE 1. Select Characteristics of the U-Rich Natural Calcite and Hanford 300 A Process Pond Sediments (<2 mm Size Fraction)

sample designation	total U (mol g^{-1})	total Cu (mol g^{-1})	total Ca (mol g^{-1})	inorg C (mol g^{-1})	depth in sample core (ft bgs)[c]
U-rich natural calcite	1.51E−06	*a*	*a*	*a*	*a*
NP4−1	1.39E−05	2.20E−04	1.09E−03	3.16E−04	1[b]
NP1−6	3.48E−06	9.36E−05	1.21E−03	9.77E−06	1[b]

[a] Not available. [b] The sediment was sampled in 1991. [c] bgs stands for below ground surface.

A U-contaminated groundwater plume that developed beneath the infiltration ponds discharges to the adjacent Columbia River. Contaminated sediment samples were obtained in 1991 from beneath the infiltration pond floor (samples prefixed NP; samples were numbered first according to arbitrary sample location and depth, e.g., NP4−1 at location 4 depth 1 foot below the original surface). The sediments were heterogeneous, with particle size ranging from clay (<2.0 μm) to 5−10 cm river cobble. Subsamples of the sediments were air-dried and sieved to obtain the < 2 mm size fraction, which was characterized for relevant chemical properties (Table 1). Total elemental composition was determined by Energy Dispersive X-ray Fluorescence Spectroscopy (KEVEX 0810A system). The method of peak analysis by this method is described in other reports (*19*, *20*). The inorganic carbon content of the sediments was determined using a Shimadzu carbon analyzer model TOC−V, SSM-5000A. Because relatively high concentrations of U(VI) resided in the fine sand-silt-clay size fraction, the spectroscopic and microscopic analyses were performed on untreated particles ranging up to 250 μm. No further treatment was applied prior to spectroscopic analysis.

Cryogenic Time-Resolved Fluorescence Spectroscopy (TRLFS) and Microscopy (TRLFISM) Measurements. The apparatus for fluorescence spectroscopic and lifetime measurements in cryostat at liquid He-temperature was described elsewhere (*15*, *16*). Briefly, a small volume of the sediment sample was pressed between a copper plate and a sapphire optical window and attached to the coldfinger of a Cryo Industries RC-152 cryogenic workstation, and the sample cell was directly exposed to the vapor flow of liquid helium at a thermostatically controlled temperature of 6 ± 1 K. Time-resolved fluorescence emission spectra were recorded with a thermoelectrically cooled Princeton Instruments PIMAX time-gated, intensified CCD camera, attached to the exit port of an Acton SpectroPro 300i double monochromator spectrograph with a slit size of 100 μm. The spectrometer offered a spectral resolution of ~2 nm (fwhm), and the time-gated

CCD camera provided a rise time of ~5 ns and a variable time delay with a minimal step of one nanosecond. The data acquisition was automated by WinSpec data acquisition software and analyzed using the commercial software package IGOR. The individual peak positions of the fluorescence spectra were obtained by fitting the spectra with the linear combination of a series of Gaussian bands using the commercial software GRAMS/A1.

The time-resolved fluorescence microscopic images and spot TRLFS measurements (TRLFISM) were recorded using a Nikon infinite-corrected 20 X Plan apochromatic objective lens on a Nikon 2000U inverted optical microscope. The sample was attached using a purpose-built sample holder attached to the coldfinger of a Cryo Industries RC-152 microscope cryostat with the sample particles sandwiched between a copper plate with indium foil linings and a sapphire window. The cryostat was then mounted on a Newport precision XY translation stage allowing sample observation within a large area. Sample excitation was achieved by a MOPO-730 pulsed laser at 415 nm incident at a small angle. After passing a 460 nm dichroic long-pass filter, the emitted light was dispersed by an Acton Research 2150i dual turret spectrograph and detected by a Roper Scientific intensified, time-gating CCD camera (512 pixels × 512 pixels). The calibrated dual-turret of the microscope allowed the acquisition of fluorescence spectra at individual spots on the optical or fluorescence image. The wavelengths of the spectrographs were calibrated using a Spectra Physics model 6033 Xenon lamp.

X-ray Diffraction and Microprobe Measurements. The < 2 mm size fraction of select sediments was analyzed by X-ray diffraction (XRD) using a Scintag XRD unit equipped with a Peltier thermoelectrically cooled detector and $Cu_{K\alpha}$ X-ray tube. Spectra were collected electronically and processed using XRD pattern processing software. Mineral phase identification was based on a comparison of the measured XRD patterns with a standard mineral powder diffraction library.

For examination by electron microprobe (EMP), sieved sediments were imbedded in epoxy and cut to provide sections through grain aggregates. The composited wafers were affixed to fused quartz slides, polished, and carbon coated. Sections were examined using a JEOL 8200 electron microprobe. Elemental abundance maps by EMP were collected by tuning wavelength-dispersive spectrometers to the characteristic X-ray fluorescence wavelengths for Cu, Si, Ca and U.

Results and Discussion

U-rich Natural Calcite (NUC). Composite time-resolved fluorescence images at a series of delay times and gate widths were acquired from the natural U-rich calcite (NUC), over an area of ~7 mm^2 by stepping the X−Y translation stage. The distribution of fluorescence (Figure 1A) showed a relatively small dynamic range, indicating that uranium was distributed more or less uniformly within the sample. Fluorescence was also relatively uniform across measurements at different delay times (Figure 1), indicating that individual contributors of the fluorescence signal were uniformly distributed. This was consistent with the results of X-ray fluorescence mapping by Kelly et al. (*1*) which indicated that uranium concentration varied only between 80 and 500 mg kg^{-1}.

Time-resolved fluorescence spectra were recorded at multiple delay times between 0 and 4 ms for bulk crystals using the 1024 element ICCD camera. At the same delay times, the spectral characteristics were similar for spectra obtained on the bulk (TRLFS) and microscope (TRLFISM) systems, regardless of the spatial location of the area examined or its relative intensity, which was presumably

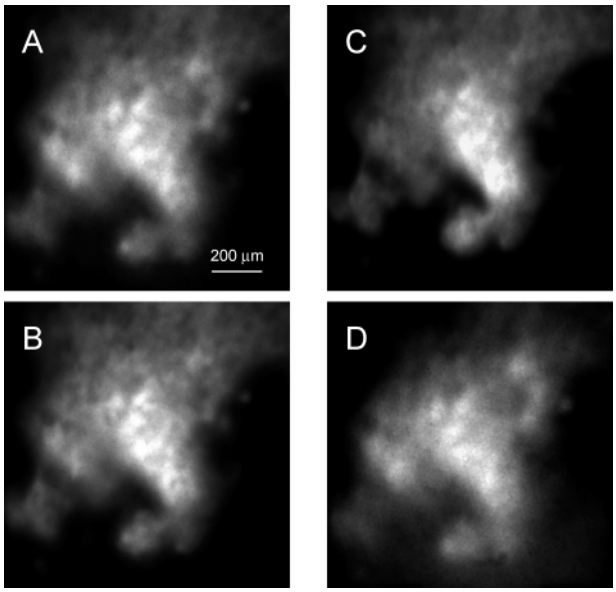

FIGURE 1. Cryogenic TRLFISM images of a natural U-rich calcite at different delay times. λ_{ex} = 415 nm. The corresponding delay and (gate width) are A: 0 μs (50 μs); B: 400 μs (50 μs); C: 1000 μs (50 μs); D: 2000 μs (50 μs). The gains of the CCD detector were adjusted so that the maximum intensities among all four images are at similar levels. Note that the spatial resolution of the images became poor at longer delay times due to the effect of multiple light scattering.

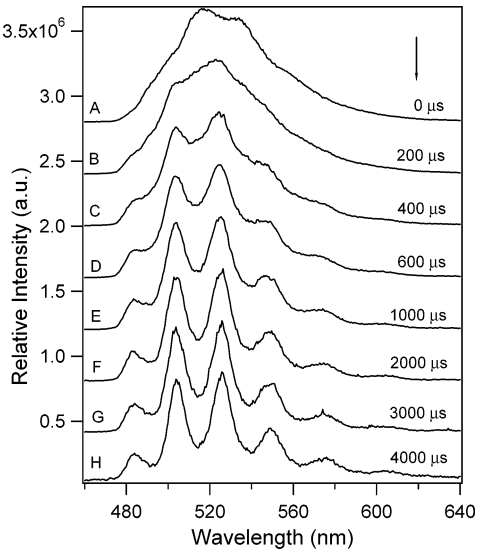

FIGURE 2. Cryogenic TRLFS spectra of a natural U-rich calcite at a series of delay times. λ_{ex} = 415 nm. The corresponding gate width are A: 50 μs; B: 50 μs; C: 50 μs; D: 50 μs; E: 50 μs; F: 50 μs; G: 200 μs; H: 400 μs in the direction of the arrow. The maximum intensities were normalized for comparison. The spectra presented in Figure 2 were acquired using the Roper Scientific THM512 ICCD camera, while spectra presented in Figures 6−8 were acquired using the THM1024:EB ICCD camera. The former has a lower quantum efficiency below 520 nm and thus showed lower spectral intensity in that region.

proportional to the relative concentration of uranium within the crystal. However, the fluorescence spectra showed significant, systematic changes as a function of the delay time. At shorter delay times, the spectra were less resolved with a spectral maximum located at ~513 nm (Figure 2), and no significant differences were observed if the delay time and/or gate width were reduced further. The spectral resolution increased as the delay time increased, and well-resolved spectra were observed after a delay of about 2 ms.

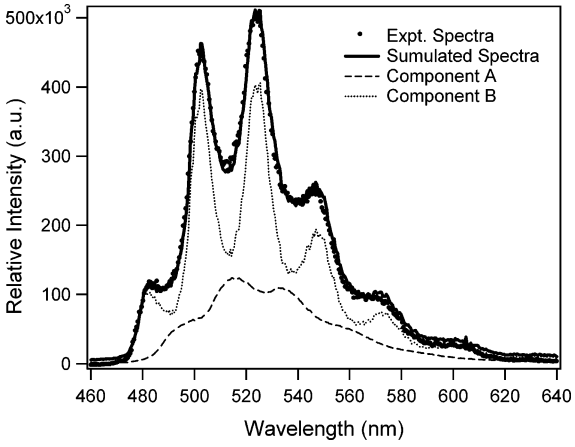

FIGURE 3. Deconvolution of the LHeT time-resolved fluorescence spectra of the U-rich natural calcite at a delay time of 1 ms and gate width of 50 μs into two unique spectral components A and B.

The spectra recorded at delay times between 2 ms and 4 ms were basically invariant, indicating that a single, long-lived uranyl species was responsible for the spectra at these delay times.

By assigning the long-delay spectrum to a single component (B), all of the spectra were definable by linear combinations of two unique spectral components, designated A and B (Figure 3; delay time of 1 ms). This analysis was applicable also to a near steady-state spectrum that was recorded using a gate width of 10 ms. The spectral component A dominated at shorter delay times, while the spectral component B dominated at longer delay times. The presence of two unique spectral components indicated that there were two characteristic uranyl coordination environments in the NUC. An accurate determination of the relative concentrations of these species would require values for their absorption coefficients at 415 nm and the corresponding fluorescence quantum yields (which we did not have).

Consistent with the spectral observations, the fluorescence decay curve for the U-rich calcite showed clear, biexponential behavior (Figure 4). A fit of the fluorescence decay data with a single-exponential function resulted in a poor agreement, while the data were well-fit with the linear combination of two exponential functions with fluorescence lifetimes of 339 μs and 92 μs, respectively. The existence of two distinct uranium species within the NUC was thus confirmed. Since the spectral component A was dominant at shorter delay times, we assigned the shorter 92 μs lifetime to this uranyl species and the longer 339 μs lifetime to species B.

Recently, Reeder et al. (*9*, *10*) studied the incorporation of uranyl into synthetic carbonates. Uranyl coprecipitated with the carbonates at a concentration of up to 1900 mg kg^{-1} for calcite and 10 000 mg kg^{-1} for aragonite. Multiple uranyl species existed in calcite grown from a high ionic strength solution at pH 7.6, while a single species dominated the calcite grown at pH 8.2 at lower ionic strength. The uranyl ion could be accommodated in the aragonite structure at a much higher concentration and involved no change in its equatorial coordination. In measurements at 77 K, uranyl in aragonite showed well-resolved fluorescence spectra with a spectral origin of ~482 nm, while the spectra of uranyl in calcite precipitated at pH 8.2 showed relatively broad fluorescence spectra with a spectral maxima at ~517 nm. The spectra of Reeder et al. (*9*, *10*) were comparable to the spectra collected from NUC. The spectrum of the longer-lived uranyl species (B) in NUC was almost identical to that of uranyl incorporated into aragonite, while the spectrum of the shorter-lived species (A) was similar to that of uranyl incorporated into synthetic calcite at pH 8.2.

Comparison of our long-lived spectra from the NUC with other results suggested that it was similar to the aqueous tricarbonate species. The liquid-helium spectrum of uranyl tricarbonate (*16*), the aqueous dicalcium-uranyl-tricarbonate, $Ca_2(UO_2)(CO_3)_3$ (*16*, *21*, *22*), the natural mineral liebigite (*16*, *21*), and the type B site in natural calcite were all very similar, implying that the equatorial coordination of uranyl in them was the same and minimally perturbed from that of the solution species.

In a previous study of the NUC using EXAFS (*1*), uranyl in a single equatorial coordination environment was observable from the analysis of the X-ray spectrum, and that was distinct from a synthetic uranyl-substituted calcite (*9*, *10*). In the NUC, the uranyl ion was coordinated by four carbonate groups in a monodentate fashion, which was essentially the same as Ca(II) in calcite, while in the synthetic calcite, the coordination was through either two bidentate and one monodentate carbonate groups or one bidentate and three monodentate carbonate groups. Our fluorescence spectra and lifetime data (Figures 2−4) indicated that uranyl in the NUC was coordinated in environments observed by EXAFS for aragonite *and* calcite. Furthermore, the fluorescence data indicated that uranyl coordination in natural calcite was similar to that in synthetic calcite. Considering that the formation of the NUC occurred at a geological time scale (13 700 y), the observation of two characteristic uranyl species suggested that the energetics of both uranyl coordination environments were similar or that there were significant fluctuations in the pH and chemical composition during its formation, similar to those observed at the laboratory time scale by Reeder et al. (*9*, *10*). Since the energy constraints on crystal growth in an aqueous medium are in part stochastic, one would not expect all of the uranyl to be coordinated in a single one of two possible configurations. The fluorescence measurements may have detected uranyl in an 'aragonite' coordination environment that comprised only a small fraction of the overall mineral sample and that was obscured by fitting uncertainty in EXAFS spectra.

There were significant differences in the spacings of the vibronic bands originating from the symmetrical stretching frequency of the aqueous uranyl ion and the fluorescence spectra for the two uranyl species in natural calcite (Figure 4 and Table 2). The peak spacing, ν_1, for uranyl in the aragonite species (B) was 812 cm^{-1}. This spacing was shorter than the aqueous uranyl ion and longer than that of the aqueous uranyl tricarbonate complex (*16*), suggesting that coordination in calcite reduced carbonate bonding to uranyl ion in the equatorial plane. The peak spacing for uranyl in the calcite species (A) was only ~719 cm^{-1}, although this value was not accurate because of peak broadness. The cause for the spectral broadness of uranyl in calcite was not clear, but such spectra were common to all U(VI)-substituted calcites analyzed by TRLFS to date.

In summary, TRLFS uranyl spectra and fluorescence lifetime data collected at bulk and microscopic scales indicated that the there were two uranyl coordination environments in the NUC. One exhibited low resolution and was similar to that of uranyl incorporated into synthetic calcite at pH 8.2 (*9*, *10*). The second was well resolved and appeared identical to uranyl incorporated into aragonite and aqueous uranyl tricarbonate.

Hanford 300 Area Pond Sediments. Sediment samples NP4−1 and NP1−6 were examined by TRLFISM and TRLFS using the procedures as applied to the NUC. As an example, Figure 5 shows the TRLFISM images at a series of delay times for sample NP4−1. The long-lived fluorescence at delays of hundreds of microseconds confirmed the presence of U(VI) in these sediments. The fluorescence distribution and the intensity varied spatially in both samples. For some large clasts, fluorescence varied spatially within the clast, and, for

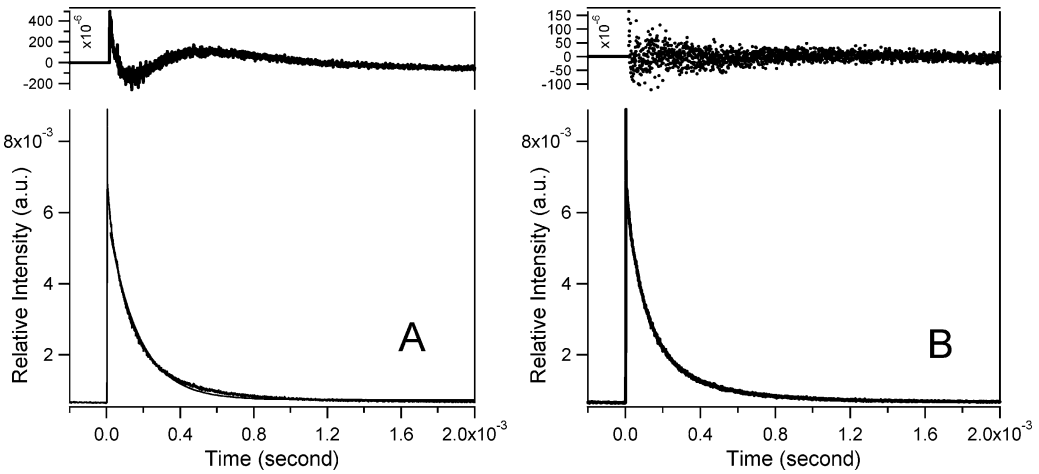

FIGURE 4. Fits of the fluorescence decay curve of U(VI) in natural calcite at LHeT by a single (A) and double (B) exponential function(s). λ_{ex} = 415 nm. The upper traces show the residuals of the fittings.

TABLE 2. Fluorescence Spectral Characteristics of U(VI) in U-Rich Natural Calcite and Hanford 300 A Process Pond Sediments[b]

sample	spectral maxima (nm)	ν_1 (f)[a] (cm^{-1})	τ at LHeT (μs)
	U-Rich Calcite		
species A	481.0, 500.0, 520.9, 543.7, 569.5	812	339
species B[a]	492.0, 511.8, 531.4, 552.0, 582.5	719	102
	NP4−1		
species A	481.6, 500.9, 521.3, 543.3, 567.2	783	422
species B[a]	493.2, 512.6, 532.7, 553.7, 577.9	743	92
	NP1−6		
species A	481.5, 501.3, 520.9, 541.9, 566.9	782	125
species B[a]	494.4, 513.0, 532.8, 556.6, 578.7	737	21

[a] The accuracy of these peak positions are poor due to the broadness of the spectral bands. [b] λ_{ex} = 415 nm.

a given set of fluorescent clasts, their relative fluorescence intensities varied as a function of delay. These observations were clear indications of the presence of multiple uranyl species and of compositional heterogeneity.

The comparison of X-ray diffraction results with results from the standard library (not shown) indicated the presence of quartz, feldspars (anorthite and albite), and calcite, with lesser amounts of augite and hornblende. Muscovite, smectite, vermiculite and chlorite were present in the silt- and clay-sized fractions. A sodium copper(II) phosphate mineral [$Na_6Cu_9(PO_4)_8$] was tentatively identified in one sediment. Aragonite or discrete uranyl minerals were not observed by XRD.

Electron beam images (Figure 6) revealed the morphology of U-bearing secondary minerals in NP sediments. Surface textures of clasts in both samples were similar (not shown), consisting of microporous, friable mineral aggregates including an aluminosilicate phase and a carbonaceous component. The NP sediments included secondary minerals coating lithic sediment clasts and abundant large precipitated clasts of secondary material (Figure 6). The heterogeneous composition of the clasts was evidence of a complex history of episodic precipitation and agglomeration. The precipitate clasts included Ca, U, Cu and Si and were compositionally heterogeneous, as illustrated by the elements' variable distribution in the single large clast in Figure 6. Although generally present at relatively low levels, Cu, U and Ca (representative of calcium carbonate) were ubiquitous and intimately associated at microscale. Within the precipitate clasts, small, μm-scale, distinct U-rich and Cu-rich inclusions

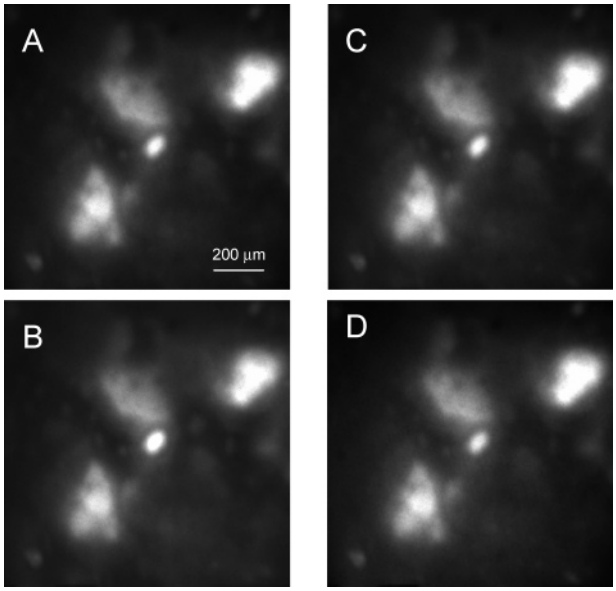

FIGURE 5. Cryogenic TRLFISM images of process pond sediment NP4−1 at different delay times. λ_{ex} = 415 nm. The corresponding delay and (gate width) are A: 0 μs (100 μs); B: 200 μs (100 μs); C: 400 μs (100 μs); D: 600 μs (100 μs). The gains of the CCD detector were adjusted so that the maximum intensities among all four images were at comparable levels. Note that the spatial resolution of the images became poor at longer delay times due to the effect of multiple light scattering.

were widespread. The distribution of Ca in similar small inclusions resulted from small discrete calcium carbonate grains. The heterogeneous distribution of Si resulted from inclusions of silicate minerals.

The TRLFS spectra of sediment samples NP4−1 and NP1−6 displayed both similarities and differences (Figures 7 and 8). At shorter delay times, both samples showed somewhat sharp spectral bands overlapped with broader spectra. This contrasted to the TRLFS spectra of the NUC at similar delay times (Figure 2) which were overwhelmed by the broad, U-bearing calcite spectra. Similar to the NUC sample, the component with sharp spectral features increased as the delay time increased. At longer delay times, the sharp, well-resolved spectra were dominant. The observed spectral features were consistent with the presence of fluorescent uranyl (*15*, *23*). For a series of randomly selected sediment particles, TRLFISM spectra were recorded for individual particles using the microscope system. The TRLFS spectra

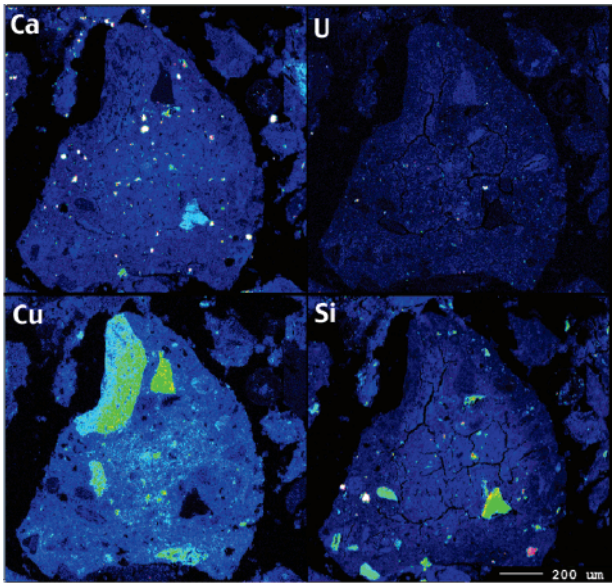

FIGURE 6. False-color elemental abundance maps from NP4−1 for Ca, U, Cu, Si. The false-color spectrum was blue-green-red-white, with the following beam-normalized, full-scale X-ray counts per second: Ca, 1000; U, 600; Cu, 300; Si, 5000. Cu was heterogeneously distributed. The large precipitate clast included aluminosilicate and other silicates (Si), and discrete inclusions of calcium carbonate (white Ca inclusions) and a uranium-rich phase (white U inclusions), but uranium and calcium were also broadly distributed at low concentration throughout.

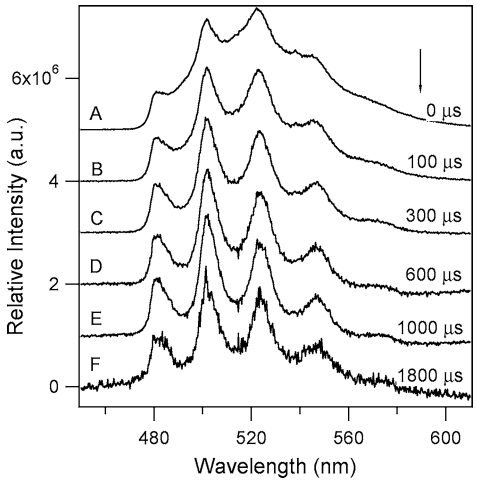

FIGURE 7. Cryogenic TRLFS spectra of NP4−1 sediment at a series of delay times. λ_{ex} = 415 nm. Gate width = 100 μs. The maximum intensities of the spectra were normalized and offset along the *Y*-axis for comparison.

for individual particles displayed similar spectra to those for the bulk sediment samples, though spectral intensities varied among the particles. The general consistency in bulk and spot spectra indicated that, while the relative concentration of fluorescent uranyl varied among the clasts or within a single clast, the overall molecular speciation in the sediments was the same.

A comparison of the TRLFS spectra of sediment NP4−1 (Figure 7) with that of the NUC (Figure 2) indicated that the spectral features of the NP4−1 at longer delay times (>600 μs) were nearly identical to those of the NUC (Figure 2 and Table 2). The NP4−1 spectra could be simulated by a linear combination of two spectral components (Figure 9), one with lower spectral resolution and a spectral maximum at ~513 nm (A) and another with high spectral resolution and a

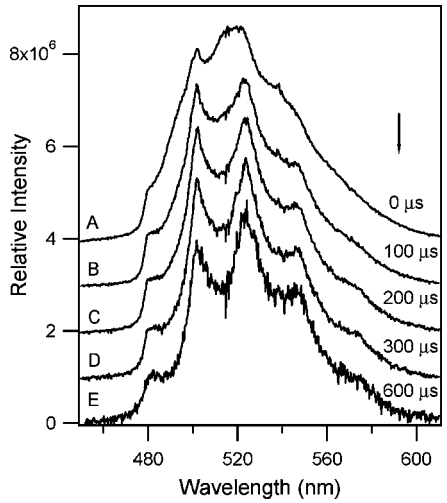

FIGURE 8. Cryogenic TRLFS spectra of NP1−6 sediment at a series of delay times. λ_{ex} = 415 nm. Gate width = 100 μs. The maximum intensities of the spectra were normalized and offset along the *Y*-axis for comparison.

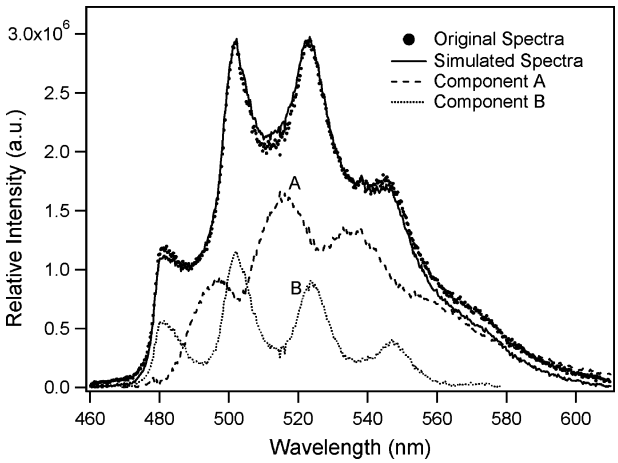

FIGURE 9. Deconvolution of the LHeT time-resolved fluorescence spectra of NP4−1 with a gate width of 10 ms and no time delay into two unique spectral components A and B.

maximum at ~501 nm (B). The fluorescence decay curves for sediment NP4−1 (not shown) could also be well fitted by a minimum of two exponential functions, yielding fluorescence lifetimes of 422 μs and 92 μs, respectively. The similarity of the fluorescence spectra and lifetimes of the uranyl species in NP4−1 to those of the NUC suggested that uranyl was incorporated in calcite and aragonite phases in the NP4−1 sediment.

The evolution of the TRLFS spectra of sediment NP1−6 as a function of delay time (Figure 8) followed a similar trend to that of both the NUC (Figure 3) and NP4−1 (Figure 7). At a delay time of 600 μs, the TRLFS spectrum of the NP1−6 sediment was dominated by sharp spectral peaks. All of the spectra could be simulated by a linear combination of two spectral components, A and B (Figure 10 panel A and Table 2) that were close to those of the corresponding components in both the NUC and the NP4−1 sediment.

However, noticeable differences existed between the fluorescence properties of the NP1−6 and NP4−1 sediments. While the fluorescence decay of sediment NP1−6 could be well fitted with two exponential functions, the resulting fluorescence lifetimes were appreciably shorter than those of the NP4−1 sediment (Table 2), suggesting the presence of fluorescence quenching. One potential cause of the quenching could be co-associated Cu and Fe ions that were

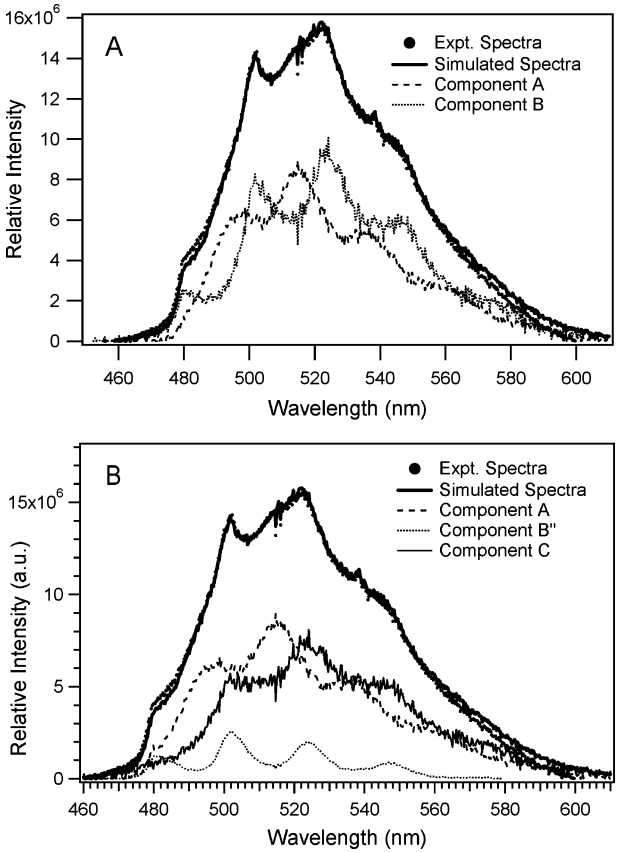

FIGURE 10. Deconvolution of the LHeT time-resolved fluorescence spectra of NP1−6 with a gate width of 10 ms and no time delay into two unique spectral components A and B (panel A) or three spectral components (panel B).

known to quench uranyl fluorescence (*24*, *25*) and to be present in the contaminated sediments in relatively high concentrations (*18*). Although the TRLFS spectra could be simulated by two spectral components (Figure 10 panel A), the spectra assigned to U-bearing aragonite differed in resolution and peak intensities from those in NUC and NP4−1 sediment. When it was assumed that NP1−6 contained the same U-bearing aragonite as in NP4−1, the spectra of component B of NP1−6 was found to be a composite of a U-bearing aragonite spectrum and a third component, C. The presence of more than two U(VI) molecular species in the NP1−6 sediment was implied.

The NP1 and NP4 samples were collected at different spatial locations and depths in the infiltration pond. NP4−1 was collected at depth of 0.25 m and NP1−6 at 1.75 m. Perhaps sediment-waste reactions caused significant differences in the pH, ion/metal composition, total carbonate concentration, and ionic strength of wastewaters at the two locations. These chemical variables are known to have significant effects on the polymorph, precipitation rate, and minor element substitution of carbonates (*26*). Significant chemical differences existed between the sediments (Table 1). More carbonate precipitation occurred from waste neutralization in sample NP4−1 (3.2%) than in the deeper NP1−6 (0.99%) sediment. Moreover, laboratory dissolution experiments with these sediments (data not shown) have revealed the presence of high soluble Mg^{2+} in sample NP4−1. The higher uranium concentration in sample NP4−1, combined with high dissolved Mg^{2+} during precipitation, could favor uranium substitution into aragonite-type coordination environments, consistent with the speciation trend observed.

The relative U(VI) fluorescence intensity of sample NP4−1 was significantly lower than the NUC, despite its 8-fold higher U(VI) content. Similarly, the fluorescence intensity of U(VI) in sample NP1−6 was disproportionately lower than what would be expected at similar concentrations in natural calcite. The weak fluorescence of sediment U(VI) may have resulted from the microscopic localization of a fluorescence quencher [i.e., Cu(I,II)] within the $CaCO_{3(s)}$ coprecipitate. This co-contaminant was present at higher concentration in the sediments than was U (Figure 6; Table 1). The weak fluorescence intensities also implied that the observed fluorescent uranyl species might only represent a portion of the entire uranium population.

The presence of similar uranyl species in the NUC and in the Hanford sediments implied that the reaction of uranyl with calcite, either through surface precipitation or coprecipitation, was partially responsible for U(VI) sorption in the sediments. However, we were puzzled by the observation that the fraction of sediment clasts displaying uranyl fluorescence (by TRLFISM) was greater than expected, given the mass concentration of calcite in these sediments. This phenomenon may be explained by the morphology of uranyl deposition. Since uranyl-bearing secondary phases including $CaCO_{3(s)}$ precipitated in a mixture of other phases (Figure 6), the sediment presented a surface in which uranyl was broadly distributed, and so was apparently rich in uranyl. Limited by the resolution of the optical microscope, fluorescence emission was observed from the entire particle. Recent work by Elzinga et al. (*3*) demonstrated that uranyl carbonate species may coprecipitate within and/or adsorb to the surface of polycrystalline calcite, potentially amplifying the observed uranyl signal.

The importance of uranyl carbonate complexes to both aqueous and surface speciation is well established (*2*, *22*, *27*−*30*). We recently demonstrated by TRLFS that uranyl tricarbonate and calcium uranyl tricarbonate complexes were the predominant uranyl species in Hanford vadose porewaters and groundwaters (*16*). Implied is that the reaction of these complexes with precipitating carbonates in the infiltration pond sediments led to their association with $CaCO_{3(s)}$ precipitates and to their distinctive TRLFS signature.

This study and others (*15*, *31*, *32*) have shown high degrees of heterogeneity and complexity in subsurface uranium speciation. In previous research, multiple uranium-bearing solid phases were observed to coexist. At the Fernald site, Morris et al. (*33*) identified autunite-like uranium phosphate precipitates, schoepite-like oxyhydroxide secondary minerals, and an ill-defined uranyl organic phase. At the Savannah River site, Hunter and Bertsch (*32*) found that most of the sediment U(VI) was associated with particulate organic material and poorly crystalline iron oxides. Multiple sorbed species have been observed also. Sorbed U(VI) was found as sodium−calcium uranyl tricarbonates and U(VI)-hydroxide or hydroxy-carbonate precipitates in California evaporation pond sediments (*31*), for example. Finally, at microscale, the reaction environment may influence the observed mode of uranium emplacement. Our previous research within Hanford's tank farms revealed the presence of intragrain uranyl silicate precipitates in a vadose zone U plume 40 m below the ground surface (*15*, *34*, *35*). Clearly, the in-ground speciation of U(VI) reflects its varied aqueous and crystal chemistry, as affected by many environmental/geochemical factors including sediment mineralogy and organic C content, waste composition, solution pH, temperature, redox conditions, water content, pore water velocity, etc.

Environmental Implications. Our TRLFS measurements showed that substituted U(VI) in calcite may exist in calcite-like or aragonite-like coordination environments and that these same molecular environments existed in U(VI)-contaminated Hanford sediments that contained variable concentrations of calcite. U(VI) was apparently entrained in

precipitating calcite in the sediments during waste-site operations, as calcite-supersaturated waste solutions migrated through in-place materials within the process ponds. Calcite supersaturation was driven by over-neutralization of wastes with NaOH to prevent metals migration to the Columbia River, absorption of atmospheric $CO_{2(g)}$, and mass-action displacement of Ca^{2+} by Na^{+} from the ion exchange complex. The extent, and possibly the rate, of calcite precipitation decreased with depth below the pond bottom as sediment−water reaction reduced the extent of calcite supersaturation.

Natural Hanford vadose zone pore waters and groundwaters are generally in equilibrium with calcite, as minor pedogenic and detrital calcite are ubiquitous sediment components at all locations. Equilibration of the sediments studied here (NP4−1 and NP1−6) with circumneutral pH electrolytes in contact with the atmosphere yielded aqueous solutions with pH between 8.0 and 8.5 that were in equilibrium with calcite (data not shown), attesting to the presence of this mineral phase and its strong control on aqueous chemistry.

The calcite-sorbed U(VI) in the Hanford sediments studied here therefore resides within a rather stable mineral environment. Its exchange with the fluid phase will be controlled by microscopic complexities of the calcite precipitate, such as its nanometer-scale depth distribution of U(VI), the U(VI) coordination environment, and nearby impurities such as Mg^{2+}, and its interfacial recrystallization rate. The U(VI) supply to percolating waters in the vadose zone will therefore be a complex kinetic process, yielding aqueous concentrations well below those sustained by discrete U(VI) precipitates. Kinetic modeling approaches are needed to forecast evolved U(VI) concentrations resulting from the dissolution and slow-redistribution of calcite-substituted U(VI) in the unsaturated environment in which these sediments currently exist. Scientifically credible calculations of this nature are essential to estimate the long-term risk of sorbed U(VI) in this vadose zone/aquifer system and its potential mobility to the nearby Columbia River.

Acknowledgments

The authors thank Dr. N. C. Sturchio at Argonne National Laboratory, Argonne, IL, for providing the uranium-rich natural calcite specimen. Discussions with Dr. S. D. Kelly also at ANL, were helpful in defining our experimental approach. This project was supported by the Hanford Remediation and Closure Science Project and by the Environmental Management Sciences Program (EMSP) managed by the U.S. DOE Office of Biological and Environmental Research (OBER). The fluorescence measurements were performed at the W.R. Wiley Environmental Molecular Sciences Laboratory, a national scientific user facility sponsored by the U.S. Department of Energy's Office of Biological and Environmental Research and located at Pacific Northwest National Laboratory. PNNL is operated for the Department of Energy by Battelle.

Literature Cited

(1) Kelly, S. D.; Newville, M. G.; Cheng, L.; Kemner, K. M.; Sutton, S. R.; Fenter, P.; Sturchio, N. C.; Spotl, C. Uranyl incorporation in natural calcite. *Environ. Sci. Technol.* **2003**, *37*, 1284−1287.

(2) Bargar, J. R.; Reitmeyer, R.; Davis, J. A. Spectroscopic confirmation of uranium(VI) − carbonato adsorption complexes on hematite. *Environ. Sci. Technol.* **1999**, *33*, 2481−2484.

(3) Elzinga, E. J.; Tait, C. D.; Reeder, R. J.; Rector, K. D.; Donohoe, R. J.; Morris, D. E. Spectroscopic investigation of U(VI) sorption at the calcite-water interface. *Geochim. Cosmochim. Acta* **2004**, *68*, 2437−2448.

(4) Xu, N.; Hochella, M. F., Jr.; Brown, G. E., Jr.; Parks, G. A. Co(II) sorption at the calcite-water interface: I. X-ray photoelectron spectroscopic study. *Geochim. Cosmochim. Acta* **1996**, *60*, 2801−2815.

(5) Reeder, R. J.; Lamble, G.; Northrup, P. A. XAFS study of the coordination and local relaxation around Co^{2+}, Zn^{2+}, Pb^{2+}, and Ba^{2+} trace elements in calcite. *Am. Minerol.* **1999**, *84*, 1049−1060.

(6) Cheng, L.; Sturchio, N. C.; Woicik, J. C.; Kemner, K. M.; Lyman, P. F.; Bedzyk, M. J. High-resolution structural study of zinc ion incorporation at the calcite cleavage surface. *Surface Sci.* **1998**, *415*, L976−L982.

(7) Rimstidt, J. D.; Balog, A.; Webb, J. Distribution of trace elements between carbonate minerals and aqueous solutions. *Geochim. Cosmochim. Acta* **1998**, *62*, 1851−1863.

(8) Meece, D. E.; Benninger, L. K. The coprecipitation of Pu and other radionuclides with $CaCO_3$. *Geochim. Cosmochim. Acta* **1993**, *57*, 1447−1458.

(9) Reeder, R.; Nugent, M.; Lamble, G.; Tait, C. D.; Morris, D. E. Uranyl incorporation into calcite and aragonite: XAFS and luminescence studies. *Environ. Sci. Technol.* **2000**, *34*, 638−644.

(10) Reeder, R.; Nugent, M.; Tait, C. D.; Morris, D. E.; Heald, S. M.; Beck, K. M.; Hess, W. P.; Lanzirotti, A. Coprecipitation of uranium(VI) with calcite: XAFS, micro-XAS, and luminescence characterization. *Geochim. Cosmochim. Acta* **2001**, *65*, 3491−3503.

(11) Min, G. R.; Edwards, R. L.; Taylor, F. W.; Recy, J.; Gallup, C. D.; Beck, J. W. Annual cycles of U/Ca in coral skeletons and U/Ca thermometry. *Geochim. Cosmochim. Acta* **1995**, *59*, 2025−2042.

(12) Russell, A. D.; Emerson, S.; Nelson, B. K.; Erez, J.; Lea, D. W. Uranium in foraminiferal calcite as a recorder of seawater uranium concentrations. *Geochim. Cosmochim. Acta* **1994**, *58*, 671−681.

(13) Shen, G. T.; Dunbar, R. B. Environmental controls on uranium in reef corals. *Geochim. Cosmochim. Acta* **1995**, *59*, 2009−2024.

(14) Stumm, W.; Morgan, J. W. *Aquatic Chemistry*, 3rd ed.; John Wiley & Sons: New York, 1996.

(15) Wang, Z.; Zachara, J. M.; Gassman, P. L.; Liu, C.; Qafoku, O.; Catalano, J. G. Fluorescence spectroscopy of U(VI)-silicate and U(VI)-contaminated Hanford sediment. *Geochim. Cosmochim. Acta* **2004**, in press.

(16) Wang, Z.; Zachara, J. M.; Yantanssee, W.; Liu, C.; Gassman, P. L.; Joly, A. G. Cryogenic laser induced fluorescence characterization of U(VI) in Hanford Vadose Zone pore waters. *Environ. Sci. Technol.* **2004**, *38*, 5591−5597.

(17) Spottl, C.; Unterwurzacher, M.; Mangini, A.; Longstaffe, F. J. Carbonate speleothems in the dry, inneralpine Vingshgau Valley, northernmost Italy: Witnesses of changes in climate and hydrology since the last glacial maximum. *J. Sed. Res.* **2002**, *72*, 793−808.

(18) (DOE) Draft Phase I. Installation Assessment of Inactive Waste-Disposal Sites at Hanford, Richland, WA. U.S. Department of Energy, 1986.

(19) Nielson, K. K. Application of direct peak analysis to energy-dispersive X-ray fluorescence spectra. *X-ray Spectrosc.* **1978**, *7*, 15−22.

(20) Nielson, K. K.; Sanders, R. W. The SAP3 Computer Program for Quantitative Multielement Analysis by Energy-Dispersive X-Ray Fluorescence, Pacific Northwest National Laboratory, 1982.

(21) Bernhard, G.; Geipel, G.; Brendler, V.; Nitsche, H. Uranium speciation in waters of different uranium mining areas. *J. Alloy Compd.* **1998**, *271−273*, 201−205.

(22) Kalmykov, S. N.; Choppin, G. R. Mixed $Ca^{2+}/UO_2^{2+}/CO_3^{2-}$ complex formation at different ionic strengths. *Radiochim. Acta* **2000**, *88*, 603−606.

(23) Rabinowitch, E.; Belford, R. L. *Spectroscopy and Photochemistry of Uranyl Compounds*; Pergaman Press: The Macmillan Company: New York, 1964.

(24) Bales, B. L.; Almgren, M. Fluorescence quenching of pyrene by copper(II) in sodium dodecyl sulfate micelles. Effect of micelle size as controlled by surfactant concentration. *J. Phys. Chem.* **1995**, *99*, 15153−15162.

(25) Stepanov, A. V.; Preobrazhenskaya, E. B.; Nikitina, S. A. Influence of temperature on the fluorescence of uranyl in frozen solutions of phosphoric and sulfuric acids in the presence of quenchers. *Radiokhmiya* **1984**, *26*, 798−803.

(26) Morse, J. W.; MacKenzie, F. T. *Geochemistry of Sedimentary Carbonates*; Elsevier: 1990.

(27) Bargar, J. R.; Reitmeyer, R.; Lenhart, J. J.; Davis, J. A. Characterization of U(VI)-carbonato ternary complexes on hematite: EXAFS and electrophoretic mobility measurements. *Geochim. Cosmochim. Acta* **2000**, *64*, 2737−2749.

(28) Davis, J. A.; Coston, J. A.; Kent, D. B.; Fuller, C. C. Application of surface complexation concept to complex mineral assemblages. *Environ. Sci. Technol.* **1998**, *32*, 2820−2828.

(29) Kato, Y.; Meinrath, G.; Kimura, T.; Yoshida, Z. A study of U (VI) hydrolysis and carbonate complexation by time-resolved laser-induced fluorescence spectroscopy (TRLFS). *Radiochim. Acta* **1994**, *64*, 107−111.
(30) Meinrath, G.; Klenze, R.; Kim, J. I. Direct spectroscopic speciation of uranium (VI) in carbonate solution. *Radiochim. Acta* **1996**, *74*, 81−86.
(31) Duff, M. C.; Morris, D. E.; Hunter, D. B.; Bertsch, P. M. Spectroscopic characterization of uranium in evaporation basin sediments. *Geochim. Cosmochim. Acta* **2000**, *64*, 1535−1550.
(32) Hunter, D. B.; Bertsch, P. M. In situ examination of uranium contaminated soil particles by micro-X-ray absorption and micro-fluorescence spectroscopies. *J. Radio. Nuclear Chem.* **1998**, *234*, 237−242.
(33) Morris, D. E.; Allen, P. G.; Berg, J. M.; Chisholm-Brause, C. J.; Conradson, S. D.; Donohoe, R. J.; Hess, N. J.; Musgrave, J. A.; Tait, C. D. Speciation of uranium in fernald spoils by molecular spectroscopic methods: Characterization of untreated soils. *Environ. Sci. Technol.* **1996**, *30*, 2322−2331.
(34) Catalano, J. G.; Heald, S. M.; Zachara, J. M.; Brown, G. E., Jr. Spectroscopic and diffraction study of uranium speciation in contaminated Vadose Aone sediments from the Hanford Site, Washington. *Environ. Sci. Technol.* **2004**, *38*, 2822−2828.
(35) Liu, C.; Zachara, J. M.; Qafoku, O.; McKinley, J. P.; Heald, S. M.; Wang, Z. Dissolution of uranyl microprecipitates from subsurface sediments at Hanford Site, USA. *Geochim. Cosmochim. Acta* **2004**, *68*, 4519−4537.

Received for review October 1, 2004. Revised manuscript received February 1, 2005. Accepted February 2, 2005.

ES048448D